Quantum-correlation-enhanced weak-field detection in an optomechanical system

Wen-Zhao Zhang,[1,*] Li-Bo Chen,[2] Jiong Cheng,[3] and Yun-Feng Jiang[4]
[1]*Beijing Computational Science Research Center (CSRC), Beijing 100193, China*
[2]*School of Science, Qingdao University of Technology, Qingdao 266033, China*
[3]*Department of Physics, Ningbo University, Ningbo 315211, China*
[4]*Department of Mechanical and Aerospace Engineering, University of California San Diego, 9500 Gilman Drive, La Jolla, California 92093, USA*

(Received 3 December 2018; published 7 June 2019)

A theoretical scheme is proposed to enhance the signal-to-noise ratio in ultrasensitive detection by quantum correlation in a composite optomechanical system. Introducing an auxiliary oscillator and treating it as an added probe for weak-field detection, the additional noise can be greatly suppressed, which may even break the standard quantum limit. A magnetic field is employed as an example to exhibit the detection capability of the scheme. The result shows that, compared with the traditional detection protocol, the scheme has a higher signal-to-noise ratio and a better detection accuracy. Furthermore, the signal intensity detection curve shows a good linearity. The results provide a promising platform for reducing the additional noise by utilizing quantum correlation in ultrasensitive detection.

DOI: 10.1103/PhysRevA.99.063811

I. INTRODUCTION

Quantum technology has a very important application prospect in ultrasensitive detection, such as mass sensor [1], force sensor [2], and quantum gyroscopes [3]. The application of quantum correlation can provide substantial enhancements for detecting and imaging weak signals in the presence of high levels of noise and loss [4–9]. For example, improving the detection signal-to-noise ratio (SNR) in quantum illumination via emitting correlation photons [4,5], enhancing the quality of ghost imaging via optical parametric amplification [6], and enhancing the precision of a position measurement via intracavity squeezing [9]. These protocols show the superiority of using quantum correlation in sensitive detection.

As a natural bridge linking the photon field and the phonon field, optomechanical systems can sense mechanical displacements optically, which provide a platform for high-precision measurements [10–13]. Optomechanical systems have been widely used in weak-field sensing due to the direct relationship of the mechanical displacement and the field intensity [10]. More importantly, as a good probe, mechanical oscillators may couple with various kinds of field, such as electric field [11], magnetic field [12], even gravitational waves [13]. Therefore, optomechanics can be used to detect these signals as an important candidate for ultrasensitive detection. Such systems demonstrate the huge susceptibility around the resonance frequency of oscillators, under the assistance of an excellent mechanical quality factor Q_m and high-sensitivity interferometric measurements [14,15]. Due to the competitive relation between photon shot noise and quantum back-action noise, the detector based on a photomechanical system has a standard quantum limit (SQL), which limits the further improvement of measurement accuracy. It has been shown that optomechanical systems can be utilized as detectors that have noise performance beyond the SQL by suppressing the additional noise with the help of quantum coherence [16–19]. Such a noise suppression scheme is achieved by quantum effects in optomechanical systems, including squeezing [13,20,21], entanglement [4,22–24], and optical high-order correlation [25].

Up to now, most of the measurement schemes are focusing on breaking the SQL [26]. However, when using quantum correlation of optical cavities to eliminate additional noises, the amplification of the signals will usually be reduced [27]. To evaluate the performance of a quantum detector based on an optomechanical system, not only the suppression of its additional noise, but also the signal amplification and the linearity of the detector response should be considered.

For the reasons given above, in this paper, an optomechanical dual-probe port scheme (OMDP) is proposed. Different from the common coherent quantum-noise cancellation schemes, which eliminate the back-action noise in measurement, we focus on breaking through the SQL by eliminating the shot noise. By using the quantum correlation between input ports, we can greatly reduce quantum noise and surpass the SQL in the measurement. In addition, the scheme can exhibit high SNR and the good ability to resist environment temperature.

The paper is organized as follows. In Sec. II we first introduce the model, then give the quantum Langevin equations and calculate the spectrum of fluctuations of the output light. After that, we give the analytic expression for the weak-field sensitivity. In Sec. III we study the additional noise and SNR in the weak-field detection. In Sec. IV we take the magnetic field as an example to show the superior capability of our scheme. In Sec. V we summarize our main conclusions.

*zhangwz@csrc.ac.cn

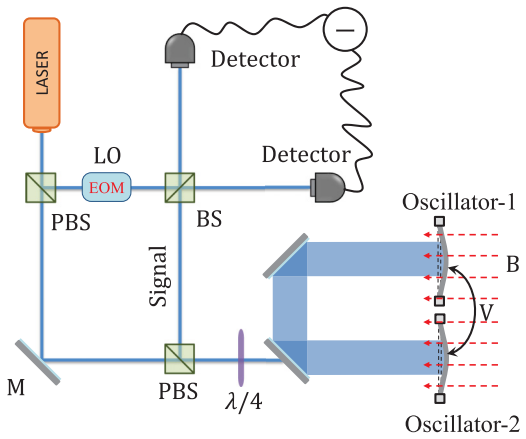

FIG. 1. The schematic diagram of a weak-field detection system. The monochromatic cavity field is coupled with two movable mirrors, and two coupled movable mirrors are used as probes to detect weak field with strength B. The laser is split into a signal beam and a local oscillator (LO). The signal beam is used to drive the cavity. The LO is phase modulated with an electro-optical modulator (EOM) and used to perform homodyne detection with the output signal beam.

II. MODEL AND HAMILTONIAN

As shown in Fig. 1, the weak-field detector is composed of a composite optomechanical system and a homodyne detection system. The Hamiltonian of the composite optomechanical system can be described as

$$H_S = \omega_c a^\dagger a + V q_1 q_2 + \sum_{j=1,2}\left[\frac{\omega_{mj}}{2}\left(p_j^2+q_j^2\right) - g_j q_j a^\dagger a\right], \tag{1}$$

where a is the bosonic operators for the optical mode with frequency ω_c. p_j and q_j are the position and momentum operator of the jth mechanical mode with frequency ω_{mj}. The single-photon coupling coefficient of the optomechanical interaction is $g_j = (\omega_c/L)\sqrt{\hbar/(2m\omega_{mj})}$. The standard continuous-wave driving can be described as $H_d = \varepsilon[a\exp(-i\omega_d t) + a^\dagger \exp(i\omega_d t)]$, where ω_d is the angular frequency of the laser and ϵ is the cavity driving strength, given by $\epsilon \equiv 2\sqrt{P\kappa_{\rm ex}/(\hbar\omega_d)}$, with P being the input power of the laser and $\kappa_{\rm ex}$ being the input rate of the cavity. V is the strength of two mechanical couplings and can be realized via a substrate-mediated interaction in a high-stress silicon nitride membrane [28]. The strength of the detection field is B, which could be electric field, magnetic field [29], and gravitational field [13] (we will give an example in Sec IV). Through the design, we can make the mechanical oscillators produce small displacement q_j in the weak field. The corresponding mechanical response coefficient of the oscillators in the weak field is ξ_j. Thus, the Hamiltonian of the mechanical oscillators surrounded by the classical field can be written as $H_b = -\sum_{j=1,2} B\xi_j q_j$.

Under strong driving conditions we can linearize the equations of motion around the steady state with $a \to \langle a\rangle + \delta a$, $p_j \to \langle p_j\rangle + \delta p_j$, $q_j \to \langle q_j\rangle + \delta q_j$. In the rotating frame with input laser frequency ω_d, the quantum Langevin equations can be obtained,

$$\delta\dot{a} = -\left(i\Delta' + \frac{\kappa}{2}\right)\delta a + \sum_{j=1,2} iG_j\delta q_j + \sqrt{\kappa_{\rm ex}}a_{\rm in} + \sqrt{\kappa_0}f_{\rm in}, \tag{2}$$

$$\delta\ddot{q}_j = -\omega_{mj}^2\delta q_j + \omega_{mj}(G_j\delta a^\dagger + G_j^*\delta a) - \omega_{mj}V\delta q_{3-j} - \omega_{mj}\gamma_j\delta p_j + \omega_{mj}F_{{\rm in},j}, \tag{3}$$

where $\Delta' = \Delta - \sum_{j=1,2} g_j\langle q_j\rangle$ denotes the driving modified detuning of the cavity, and $G_j = g_j\langle a\rangle$ denotes the linearized coupling. κ_0 denotes the loss rate inside the cavity. The total cavity loss rate can be written as $\kappa = \kappa_{\rm ex} + \kappa_0$. $F_{{\rm in},j} = \sqrt{\gamma_j}P_{{\rm th},j} + \xi_j B$ is the input term of the mechanical oscillator, $P_{{\rm th},j}$ is the noise operator. Introducing the Fourier transformation, the operator dynamic of the system in frequency domain becomes

$$\delta a(\omega) = \chi_c[iG_1\delta q_1(\omega) + iG_2\delta q_2(\omega) + \sqrt{\kappa_{\rm ex}}a_{\rm in}(\omega) + \sqrt{\kappa_0}f_{\rm in}(\omega)], \tag{4}$$

$$\delta q_j(\omega) = \chi_{mj}[G_j\delta a^\dagger(-\omega) + G_j^*\delta a(\omega) - V\delta q_{3-j}(\omega) + F_{{\rm in},j}(\omega)], \tag{5}$$

where $\chi_c = [i(\Delta'-\omega) + \kappa/2]^{-1}$ and $\chi_{mj} = [\omega_{mj} - \omega^2/\omega_{mj} - i\gamma_j\omega/\omega_{mj}]^{-1}$ are susceptibilities of cavity and mechanical oscillators, respectively. For the slow varying field or the steady field, the input term can be written as $F_{{\rm in},j}(\omega) = \sqrt{\gamma_j}P_{{\rm th},j}(\omega) + \delta(\omega)\xi_j B$. Using the standard input-output relation $O_{\rm out} = \sqrt{\kappa_{\rm ex}}O - O_{\rm in}$ and considering the homodyne measurement shown in Fig. 1, we have the output operator

$$\begin{aligned} M_{\rm out}(\omega) &= i[a_{\rm out}^\dagger(-\omega)e^{-i\theta} - a_{\rm out}(\omega)e^{i\theta}] \\ &= A(\omega)a_{\rm in}(\omega) + B(\omega)a_{\rm in}^\dagger(-\omega) \\ &\quad + A_0(\omega)f_{\rm in}(\omega) + B_0(\omega)f_{\rm in}^\dagger(-\omega) \\ &\quad + C(\omega)F_{{\rm in},1}(\omega) + D(\omega)F_{{\rm in},2}(\omega), \end{aligned} \tag{6}$$

where θ is a controllable phase which can reduce the additional noise and has been studied in Ref. [30]. For simplicity, we choose $\theta = 0$ and $G_j = G$, the coefficients in Eq. (6) can be written as

$$A(\omega) = i(1-\kappa\chi_c) + \frac{i\kappa\chi_c(|G|^2\chi_c + G^{*2}\chi_c^\dagger)(2V\chi_{m1}\chi_{m2} - \chi_{m1} - \chi_{m2})}{D_e},$$

$$B(\omega) = -i(1-\kappa\chi_c^\dagger) + \frac{i\kappa\chi_c^\dagger(|G|^2\chi_c^\dagger + G^{*2}\chi_c)(2V\chi_{m1}\chi_{m2} - \chi_{m1} - \chi_{m2})}{D_e},$$

$$A_0(\omega) = \frac{\sqrt{\kappa_{ex}\kappa_0}\chi_c}{D_e}[(V^2\chi_{m1}\chi_{m2} - 1) + 2i|G|^2\chi_c^\dagger(2V\chi_{m1}\chi_{m2} - \chi_{m1} - \chi_{m2})],$$

$$B_0(\omega) = \frac{\sqrt{\kappa_{ex}\kappa_0}\chi_c^\dagger}{D_e}[(V^2\chi_{m1}\chi_{m2} - 1) - 2i|G|^2\chi_c(2V\chi_{m1}\chi_{m2} - \chi_{m1} - \chi_{m2})],$$
$$C(\omega) = \frac{i\sqrt{\kappa}(G\chi_c + G^*\chi_c^\dagger)(V\chi_{m1}\chi_{m2} - \chi_{m1})}{D_e},$$
$$D(\omega) = \frac{i\sqrt{\kappa}(G\chi_c + G^*\chi_c^\dagger)(V\chi_{m1}\chi_{m2} - \chi_{m2})}{D_e}. \tag{7}$$

The denominator $D_e = i(V^2\chi_{m1}\chi_{m2} - 1) + |G|^2(\chi_c - \chi_c^\dagger)(2V\chi_{m1}\chi_{m2} - \chi_{m1} - \chi_{m2})$, the cavity susceptibility satisfies the relationship $\chi_c^\dagger = \chi_c^*(-\omega)$.

III. WEAK-FIELD DETECTION

Assuming that the two mechanical oscillators have the same response rate $\xi_1 = \xi_2 = \xi$, Eq. (6) can be rewritten as

$$M_{\rm out}(\omega) = A(\omega)a_{\rm in}(\omega) + B(\omega)a_{\rm in}^\dagger(-\omega) + A_0(\omega)f_{\rm in}(\omega) + B_0(\omega)f_{\rm in}^\dagger(-\omega) + C(\omega)\sqrt{\gamma_1}P_{{\rm th},1}(\omega)$$
$$+ D(\omega)\sqrt{\gamma_2}P_{{\rm th},2}(\omega) + [C(\omega) + D(\omega)]\delta(\omega)\xi B. \tag{8}$$

According to Eq. (8), the coefficient of the weak-field intensity (B) directly represents the amplification characteristic from the detection signal to the output signal. Therefore, the amplification coefficient of the system can be defined as $A_p = |C(\omega) + D(\omega)|$. Analogously, the other items without B in the output operator can be regarded as noise. To obtain the relationship between the output signal and the noise, Eq. (8) can be rewritten as

$$\frac{M_{\rm out}}{C(\omega) + D(\omega)} = \frac{A(\omega)}{C(\omega) + D(\omega)}a_{\rm in}(\omega) + \frac{B(\omega)}{C(\omega) + D(\omega)}a_{\rm in}^\dagger(-\omega) + \frac{A_0(\omega)}{C(\omega) + D(\omega)}f_{\rm in}(\omega)$$
$$+ \frac{B_0(\omega)}{C(\omega) + D(\omega)}f_{\rm in}^\dagger(-\omega) + \frac{C(\omega)\sqrt{\gamma_1}P_{{\rm th},1} + D(\omega)\sqrt{\gamma_2}P_{{\rm th},2}}{C(\omega) + D(\omega)} + \delta(\omega)\xi B, \tag{9}$$

thus the additional noise can be defined as

$$F_{\rm add} = \frac{A(\omega)}{C(\omega) + D(\omega)}a_{\rm in}(\omega) + \frac{B(\omega)}{C(\omega) + D(\omega)}a_{\rm in}^\dagger(\omega) + \frac{A_0(\omega)}{C(\omega) + D(\omega)}f_{\rm in}(\omega) + \frac{B_0(\omega)}{C(\omega) + D(\omega)}f_{\rm in}^\dagger(-\omega)$$
$$+ \frac{C(\omega)\sqrt{\gamma_1}P_{{\rm th},1} + D(\omega)\sqrt{\gamma_2}P_{{\rm th},2}}{C(\omega) + D(\omega)}. \tag{10}$$

The first four terms describe the input noise from the cavity, resulting in the SQL [31]. The last term describes the thermal noise from the mechanical environment. According to the expression in Eqs. (7), we can find that $A(\omega)$, $B(\omega)$, $A_0(\omega)$, $B_0(\omega)$, $C(\omega)$, and $D(\omega)$ contain coherent terms caused by coupling V, i.e., $V\chi_{m1}\chi_{m2}$. Thus, one may reduce $F_{\rm add}$ by appropriately modulating the coupling rate V. From the general definition of the noise spectrum, we have

$$S_{\rm add}(\omega) = \tfrac{1}{2}[S_{FF}(\omega) + S_{FF}(-\omega)], \tag{11}$$

where $S_{FF}(\omega) = \int d\omega' \langle F_{\rm add}(\omega)F_{\rm add}(\omega')\rangle$. The vacuum radiation input noise $a_{\rm in}$ and internal noise operator $f_{\rm in}$ satisfies a δ-correlation function. The operator $P_{{\rm th},j}(\omega)$ describes the input thermal noise. Under Born-Markov approximation, we have $\langle P_{{\rm th},j}^\dagger(\omega)P_{{\rm th},j}(\omega')\rangle \approx n_{{\rm th},j}\delta(\omega - \omega')$, where $n_{{\rm th},j} = [\exp(\hbar\omega_{m,j}/k_BT) - 1]^{-1}$ describes the equivalent thermal occupation. The additional noise spectrum density becomes

$$S_{\rm add}(\omega) = \frac{1}{2}\left[\left|\frac{A(\omega)}{E(\omega)}\right|^2 + \left|\frac{B(\omega)}{E(\omega)}\right|^2 + \left|\frac{A_0(\omega)}{E(\omega)}\right|^2 + \left|\frac{B_0(\omega)}{E(\omega)}\right|^2\right]$$
$$+ S_{\rm th}(\omega), \tag{12}$$

where $E(\omega) = C(\omega) + D(\omega)$, $S_{\rm th}(\omega) = \gamma_1 n_{\rm th1}|C(\omega)/E(\omega)|^2 + \gamma_2 n_{\rm th2}|D(\omega)/E(\omega)|^2$. In Eq. (12), the first four terms describe the noise from the cavity. The internal loss of the cavity usually leads to the effective loss of the information, which is not advantageous for many experiments [26]. Figure 2 show how the internal loss acts on the additional noise in detection. In Fig. 2(a), the input rate of the cavity ($\kappa_{\rm ex}$) is fixed. The minimum value of additional noise in detection will increase with the increase of the internal cavity loss rate. Similar conclusions can also be obtained in Fig. 2(b). When the total dissipation rate (κ) is fixed, the minimum value of additional noise will also increase with the increase of the proportion of internal loss. It means that both the absolute and

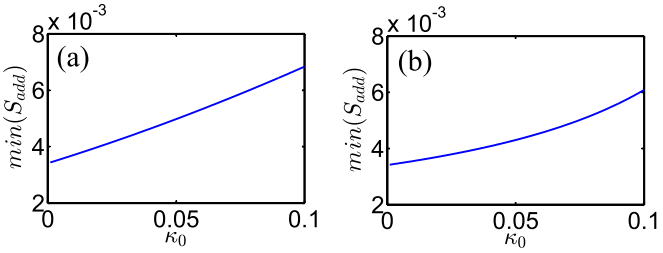

FIG. 2. The minimal additional noise as a function of κ_0. (a) $\kappa_{\rm ex}/\omega_m = 0.2$. (b) $\kappa/\omega_m = 0.2$. Other parameters are $G/\omega_m = 0.03$, $\gamma_1 = \gamma_2 = 10^{-5}\omega_m$, $V/\omega_m = 0.2$, $\omega_m = 5 \times 10^6$ Hz, and $n_{\rm th} = 10$.

relative value of internal loss rate have a negative effect on the detection. Thus, internal loss needs to be reduced in detection. In experiments, an "overcoupled" cavity [26,32] can usually be used to build the optomechanics, the external loss of which is the dominant cavity loss ($\kappa \approx \kappa_{ex} \gg \kappa_0$).

In the following discussion, the impact of internal loss is neglect. Under the condition $\Delta' = \omega_{m,j} = \omega_m$, $\kappa_0 = 0$, and $G_j = G$, we have

$$S_{add}(\omega) = \left| \frac{1 - V^2\chi_{m1}\chi_{m2}}{2V\chi_{m1}\chi_{m2} - \chi_{m1} - \chi_{m2}} \frac{-i[\omega^2 + (\kappa/2 - i\omega)^2]}{2\sqrt{\kappa}(\kappa/2 - i\omega)G} + \frac{2(\kappa - i\omega_m)}{\sqrt{\kappa}(\kappa - 2i\omega_m)}G \right|^2 + S_{th}(\omega). \quad (13)$$

This should be compared to the result of the standard optomechanical scenario [26]

$$S_{add1}(\omega) = \left| \frac{-i[\omega^2 + (\kappa/2 - i\omega)^2]}{2\chi_{m1}\sqrt{\kappa}(\kappa/2 - i\omega)G} + \frac{2(\kappa - i\omega_m)G}{\sqrt{\kappa}(\kappa - 2i\omega_m)} \right|^2 + \gamma_1 n_{th1}, \quad (14)$$

with its familiar shot-noise term scaling as $1/G^2$ and the back-action term scaling as G^2. The SQL of the standard optomechanical scheme ($S_{SQL,1}$) and our scheme ($S_{SQL,2}$) can be obtained by minimizing S_{add1} and S_{add} with respect to G at $T = 0$. The minimal value of $S_{SQL,1}(\omega)$ and $S_{SQL,2}(V = 0, \omega)$ can be obtained at $\omega = \omega_m$. To investigate the noise limit of our scheme, we define two SQL proportion factors,

$$R_1(\omega) = \frac{S_{SQL,2}(\omega)}{S_{SQL,1}(\omega = \omega_m)}, \quad (15)$$

$$R_2(\omega) = \frac{S_{SQL,2}(\omega)}{S_{SQL,2}(V = 0, \omega = \omega_m)}, \quad (16)$$

R_1 is defined to compare the SQL of OMDP with the standard optomechanical scheme. $R_1 < 1$ denotes our scheme beyond the SQL of the standard optomechanical scheme. R_2 is defined to compare the SQL of OMDP with and without mechanical interaction. $R_2 < 1$ denotes our scheme with mechanical interaction beyond the SQL of that without mechanical interaction. The comparison of SQL with different parameters are shown in Fig. 3. The white-dashed line denotes $R_j = 1$. The additional noise exhibits a minimal value at the specific frequency in the dark area. Under the condition $\{G_j, \gamma_{m,j}\} \ll \omega_m$, this optimized frequency can be obtained i.e., $\omega_{eff} \approx \sqrt{\omega_m(\omega_m + V)}$. This frequency can be obtained by the diagonalization of the two oscillators [33]. The low frequency part will be decoupled from the magnetic field under the given parameters. It is shown that the SQL of our scheme can go beyond the SQL of the standard optomechanical scheme and OMDP without mechanical interaction. The corresponding optimized parameters area is between the white-dashed lines in the figure. At the optimized frequency ω_{eff}, R_j are very small, where R_1 is on the order of 10^{-7} and R_2 is on the order 10^{-5}. In Fig. 3(a), when mechanical interaction $V = 0$, the SQL of OMDP is a little lower than the standard optomechanical scheme in the frequency area $\omega \in [0.9\omega_m, 1.1\omega_m]$. A similar result of R_2 can be found in Fig. 3(b). The SQL of OMDP may reach a rather lower level with the help of mechanical interaction.

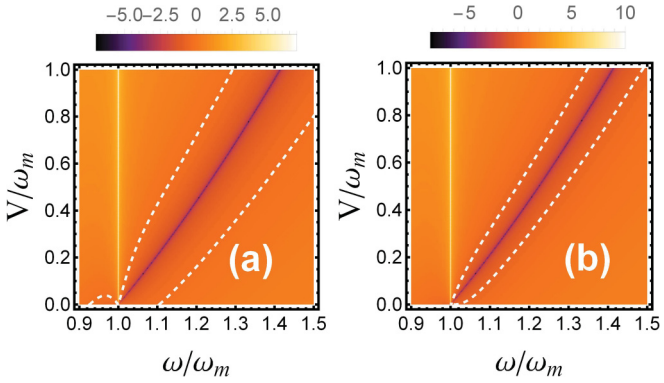

FIG. 3. R_j as a function of frequency ω and mechanical coupling V (on a logarithmic scale). White-dashed line denotes $R_j = 1$. (a) and (b) Density plots of R_1 and R_2, respectively. The parameters are $\kappa/\omega_m = 0.1$, $\gamma_1 = \gamma_2 = 10^{-5}\omega_m$, $\omega_m = 5 \times 10^6$ Hz.

The above calculation is discussed under the condition $T = 0$. However, in realistic situations, the thermal noise should be taken into account. Note that, in our system, the addition of detection ports does not increase the effective thermal noise. Instead, it reduced the thermal noise slightly. According to the expression of $S_{th}(\omega)$ under Eq. (12), the thermal noise is only half of the original one [$S_{th}(\omega) = \gamma_1 n_{th1}/2$] when the parameters of the oscillators are identical. That is because the quantum correlation of different thermal oscillators can be ignored.

The additional noise spectrum and amplification spectrum are shown in Fig. 4. There is a minimal value of additional noise at the frequency ω_{eff}. In addition, lower additional noise requires a larger value of V. When $V = 0$, the minimal value of additional noise is almost the same as the one under the single detection port (marked as "single"). The same result can be found in the amplification spectrum, however, the amplification rate increases monotonically as the parameter V increases.

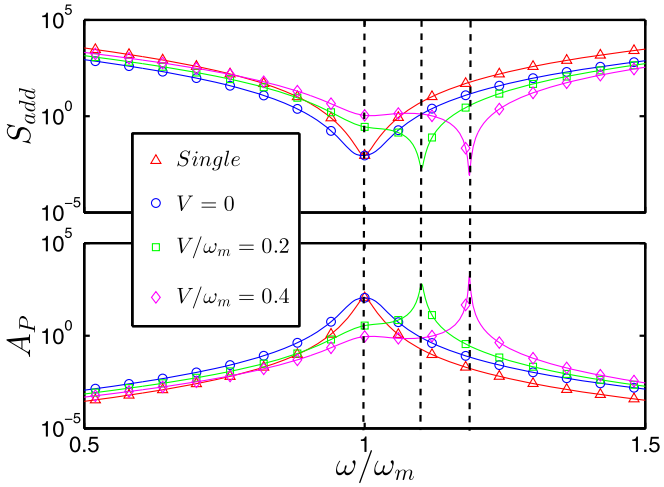

FIG. 4. Additional noise and amplification coefficient as a function of frequency ω. $G/\omega_m = 0.03$, $\kappa/\omega_m = 0.1$, $n_{th} = 10$, $\Delta\omega/\omega_m = 0$, $\gamma_1 = \gamma_2 = 10^{-5}\omega_m$, $\omega_m = 5 \times 10^6$ Hz.

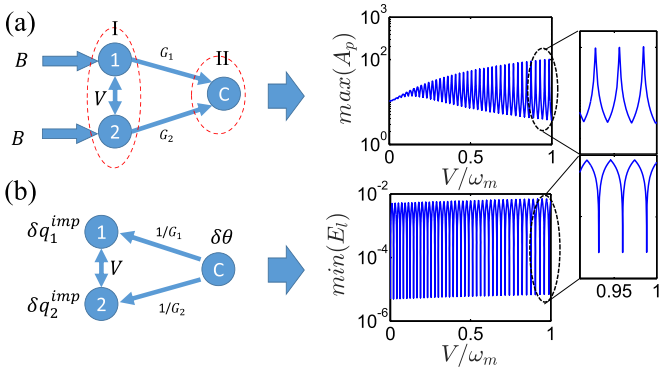

FIG. 5. (a) The diagram of "positive effect" and the corresponding optimum amplification coefficient $\max[A_p(\omega)]$ as a function of V. (b) The diagram of "negative effect" and the corresponding optimum elimination coefficient $\min[E_l(\omega)]$ as a function of V. The parameters are the same as that in Fig. 4.

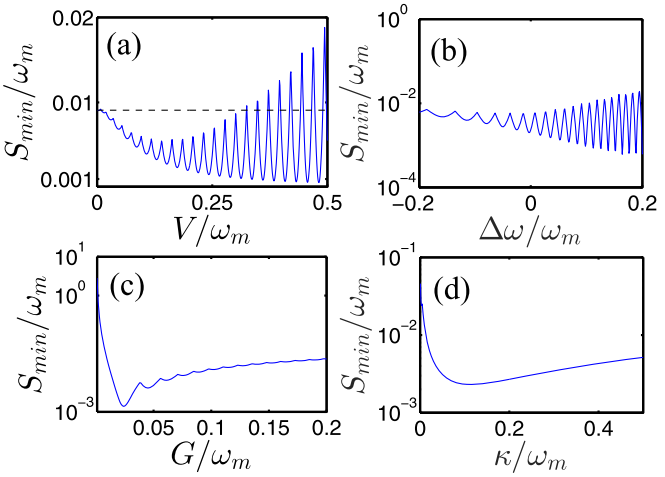

FIG. 6. (a) The minimal additional noise as a function of V. (b) The minimal additional noise as a function of $\Delta\omega$. (c) The minimal additional noise as a function of G. (d) The minimal additional noise as a function of κ. Other parameters are $V/\omega_m = 0.2$, $G/\omega_m = 0.03$, $\kappa/\omega_m = 0.1$, $\Delta\omega/\omega_m = 0$, $\gamma_1 = \gamma_2 = 10^{-5}\omega_m$, $\omega_m = 5 \times 10^6$ Hz, and $n_{\rm th} = 10$.

Figure 5 explains the noise reduction and signal amplification in our scheme. As shown in Fig. 5(a), the signal to detect is transformed into the displacement of the mechanical modes through the response of mechanical detection ports. Then these displacements are transformed into the change of the optical mode through the optomechanical coupling for further detection. Since we have two input ports (two mechanical oscillators), coherent amplification will occur in the first signal transition, i.e., region I in the figure. In the second signal transition, coherent amplification will also occur due to the interaction between two coupled mechanical oscillators and the same cavity, i.e., region II in the figure. In these two cascade coherences, the signal can be amplified greatly compared to the original scheme. According to the definition of $A_p(\omega)$, we can obtain $A_p \propto \{|i(V^2\chi_{m1}\chi_{m2} - 1) + (\chi_c - \chi_c^\dagger)[|G_1|^2\chi_{m1} + |G_2|^2\chi_{m2} - 2V(G_1^*G_2 + G_1G_2^*)\chi_{m1}\chi_{m2}]|\}^{-1}$. The first term denotes the coherent amplification of region I. The second term denotes the coherent amplification of region II. Large A_p can be obtained under an appropriate value of $\{V, G_1, G_2\}$.

We name the coherence process from mechanical oscillators to cavity as "positive effect," which makes the optimal amplification factor oscillate with the changing of V. It is difficult to analytically show the oscillation relationship between $\max[A_p(\omega)]$ and V, because coupling can lead to a shift effect of effective frequency. Therefore, we show this positive effect numerically in the figure. The amplitude of $\max[A_p(\omega)]$ increases along with the increasing of V. A good enhancement can be realized under an appropriate value of V.

Traditionally, quantum noise cancellation schemes are based on back-action noise reduction, while our scheme focuses on shot-noise reduction. According to Ref. [26], the optical phase readout ($\delta\theta \sim 1/\sqrt{N}$) induces an imprecision in the q measurement, where $\delta q^{\rm imp} \sim \kappa\delta\theta/G$, which is defined as shot noise.

As shown in Fig. 5(b), the imprecision in the displacement readout of two coupled mechanical oscillators are subject from the same cavity. Thus, shot noise in our system describes the imprecise noise from the cavity to mechanical oscillators. This process is an inverse process of positive effect (the coherence process from mechanical oscillators to cavity), which can be regarded as "negative effect." The strength of negative effect can be expressed by parameter $E_l(\omega) = [1 - V^2\chi_{m1}\chi_{m2}]/[2V\chi_{m1}\chi_{m2} - \chi_{m1} - \chi_{m2}]$ in Eq. (13). Comparing with the amplification of positive effect $A_p(\omega) \propto |(V^2\chi_{m1}\chi_{m2} - 1)^{-1}|$, $E_l(\omega)$ will naturally lead to the reduction of negative effect. As shown in Fig. 5(b), we plot $\min[E_l(\omega)]$ as a function of V. It can be clearly seen that $\min[E_l(\omega)]$ and $\max[A_p(\omega)]$ show the opposite oscillation trend. This is why we need to reduce shot noise rather than back-action noise in our scheme.

To study the the relationship between additional noise and adjustable parameters, we plot Fig. 6. As shown in Fig. 6(a), the minimal additional noise $S_{\rm min}$ exhibits an oscillating decrease along with the increase of V. The oscillating amplitude also gets larger in the meantime. This is consistent with the analysis of Eq. (10) that the coupling between two oscillators contribute to the interference cancellation of the additional noise. However, a larger V does not guarantee a better result. Negative effect of detection like destructive interference also exist. For example, when $V = 0.47\omega_m$, the minimum noise $S_{\rm min} = 0.015$, which is larger than the case without mechanical interaction. Thus, in order to suppress the additional noise, we need to choose an appropriate coupling coefficient. As shown in Fig. 6(b), we plot the minimal additional noise with frequency difference $\Delta\omega = \omega_{m1} - \omega_{m2}$. Similar to the conclusion of Fig. 6(a), the additional noise shows a coherent effect due to mechanical coupling. The frequency difference $\Delta\omega$ affects the value of χ_{m2} and thus affects the coherence term, i.e., $V\chi_{m1}\chi_{m2}$. Moreover, the amplitude of the curve increases with the increasing of $\Delta\omega$. In experimental realization, to obtain a larger mechanical coupling, we usually need to set $\Delta\omega \approx 0$ [28]. Figure 6(c) shows the effect of linearized coupling strength on minimum additional noise. The minimum additional noise $S_{\rm min}$ has a valley value along with the increase of the linear coupling coefficient. When $G < 0.02\omega_m$, $S_{\rm min}$ decreases with the increasing of G. When

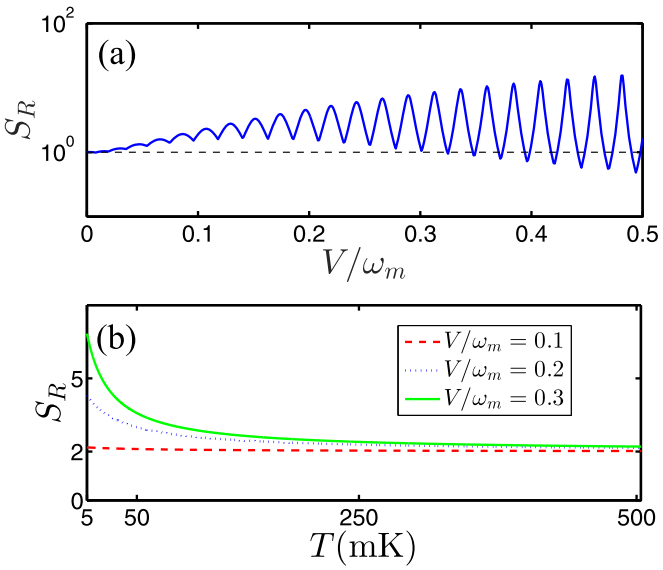

FIG. 7. (a) S_R as a function of coupling V, where environment temperature $T = 1$ mK. (b) S_R as a function of environment temperature T with different coupling. Other parameters are the same as that in Fig. 4.

$G > 0.02\omega_m$, $S_{\min}$ increases with the increasing of G. This phenomenon is due to the dependent relationship between the back-action noise and the shot noise, which has been studied recently [2]. As shown in Fig. 6(d), we plot $S_{\min}$ as a function of κ. Similar to the conclusion of Fig. 6(c), due to the competitive relationship between the back-action noise and the shot noise, $S_{\min}$ has a minimum value.

A quantum detector based on an optomechanical system should not be evaluated only by its additional noise suppression. Instead, signal-to-noise ratio (SNR) and the linearity of the detector response should also be taken into account. According to the standard SNR definition and the expression of Eq. (9), we have $\mathrm{SNR}(\omega) = \xi^2 B^2 / S_{\mathrm{add}}(\omega)$, where ξ and B are constant in our analysis. Thus, we can easily learn the characteristics of SNR from the additional noise. To investigate the enhancement of SNR in our scheme under finite temperature, we define the proportion factor $S_R = \mathrm{SNR}(\omega_{\mathrm{eff}})/\mathrm{SNR}_0$, where SNR_0 is the maximum SNR of the standard optomechanical scenario. $S_R > 1$ indicates that in the presence of the coupling, the SNR is better than the case without mechanical interaction, and vice versa. As shown in Fig. 7(a), at low temperature regime, our scheme exhibits a remarkable advantage by choosing an appropriate coupling rate, which is consistent with the analysis in Fig. 6(a). This is because the definition of additional noise is a relative noise [2,26], which includes the proportion of signal amplification. As shown in Fig. 7(b), with the increase of temperature, S_R gradually decreases to a constant 2. When the environment temperature is high enough, the value of S_R depends only on the thermal noise of the mechanical oscillators. In the previous analysis we know that our system can reduce the effective thermal noise by half, that is why the final S_R will approach constant 2. To fully take advantage of the mechanical correlation for enhancing SNR and reducing additional noise, an appropriate mechanical coupling rate is important. Although our scheme has a great advantage in resisting noise, it is still necessary to keep the detector in a low temperature environment.

In our scheme, the key to enhancing the detection effect is the coherent interaction between two mechanical oscillators. The larger the coupling strength, the more obvious the detection enhancement effect is. However, strong coupling between mechanical oscillations are difficult to realize in the experiment. Recently, various theoretical and experimental schemes have been proposed to overcome this difficulty [34–42], which provide the possibility of feasibility for our scheme. Strong dynamic coupling between two mechanical resonators can be physically realized by using a piezoelectric transducer [37–39]. The mechanical coupling parameter is proportional to gate voltage and can be tuned in micro- (nano-) oscillator systems [38,39]. The mechanical oscillators can even achieve super-strong coupling through the indirect effect of the light field [41,42]. The coupling strength of silicon oscillators on the thick device layer of a SOI wafer can reach the magnitude of the oscillator's intrinsic frequency through the indirect interaction of the optical spring [42]. Thus, under the existing experimental conditions, we can achieve the required coupling strength by adding direct coupling devices (piezoelectric transducer) or indirect coupling devices (optical spring). Note that the indirect additional mechanical coupling system must be in a dimension that does not change the Hamiltonian of our model. (It can be in different optical polarization, frequency or vector direction, etc.)

IV. APPLICATION EXAMPLE: WEAK MAGNETIC FIELD DETECTION

In this section, taking magnetic field as an example, our system can be regarded as a magnetometer. The magnetic field is responsive to the mechanical oscillators with surface charge [43]. As shown in Fig. 1, oscillators 1 and 2 are simultaneously used as probes for magnetic field. Different strengths of the magnetic field will cause different displacements of the oscillators. Assuming the magnetic field is homogeneous, the corresponding Hamiltonian can be written as $H_b = -\sum_{j=1,2} B\xi_j q_j$, where B represents the intensity of the magnetic field, $\xi_j = IL$ denotes the constant related to the surface charge characteristics, I denotes surface current of the mechanical oscillators, and L denotes the size of the oscillators.

In a macro-optomechanical system, mechanical frequency $\omega_m = 2\pi \times 10.56$ MHz, $\gamma_m = 2\pi \times 32$ Hz, mechanical diameter $d = 15$ μm [32]. The SNR and the precision of the detection system has been shown in Fig. 8. Consistent with the conclusion of the previous section, the optimal detection frequency is ω_{eff}. The SNR of the field detector can reach the order 10^6 with $B = 10^{-13}$ T. The corresponding output photon number is $n = 1.7 \times 10^6$. With the increase of field strength, the SNR increases significantly. In Fig. 8(b) we investigate the detection accuracy and response characteristics of the detector. Here we define that the detection accuracy is the intensity of magnetic field when SNR is equal to 1. It can be found that, under the given parameters, the detection accuracy can reach 8.4×10^{-20} T. This accuracy can be further improved by increasing the response rate ξ_j. Besides, there is an obvious linearity relationship between SNR and input field strength B. In our calculation, SNR is a linear

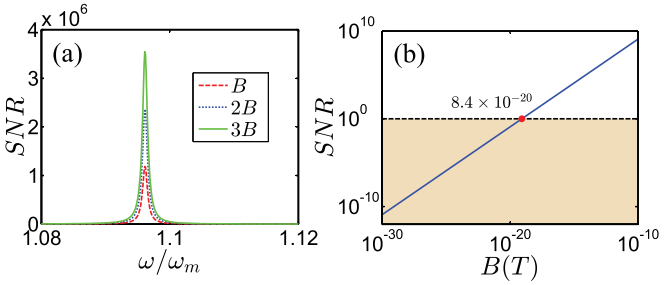

FIG. 8. (a) SNR spectrum with different magnetic field intensity. (b) SNR(ω_{eff}) as a function of magnetic field intensity. $B = 10^{-13}$ T, $I = 10$ μA, $V/\omega_m = 0.2$, $\kappa/\omega_m = 0.1$, $\gamma_1 = \gamma_2 = 2\pi \times 32$ Hz, $\omega_m = 2\pi \times 10.56$ MHz, $T = 1$ mK.

function of the output photon strength. Therefore, SNR can be used directly to indicate the intensity of output signal. This weak-field detection system satisfies all requirements we have mentioned in Sec. I.

V. CONCLUSION

In conclusion, the weak-field dual-port detection protocol can effectively suppress the additional noise and even break through the standard quantum limit of standard optomechanical protocols [26]. By using the quantum correlation between mechanical oscillators and selecting the appropriate coupling strength, we can greatly reduce the noise without weakening the signal and achieve a high SNR. Under the existing experimental conditions, we take the weak magnetic field as an example to evaluate the performance of our scheme. Under the given parameters in Ref. [32], the simulated detection accuracy can reach 8.4×10^{-20} T. The detector also has a high SNR and a good linear response curve. Our scheme provide a promising application of the optomechanical system in quantum weak-field detection.

ACKNOWLEDGMENTS

Project supported by the National Natural Science Foundation of China (Grants No. 11704026, No. 11304174, No. 11704205, and No. U1530401), the China Postdoctoral Science Foundation funded project (Grant No. 2018T110039), the Natural Science Foundation of Shandong Province (Grant No. ZR2013AQ010), and the Natural Science Foundation of Ningbo (Grant No. 2018A610199).

[1] Y. He, Appl. Phys. Lett. **106**, 121905 (2015).
[2] W.-Z. Zhang, Y. Han, B. Xiong, and L. Zhou, New J. Phys. **19**, 083022 (2017).
[3] P. Kok, J. Dunningham, and J. F. Ralph, Phys. Rev. A **95**, 012326 (2017).
[4] S. Barzanjeh, S. Guha, C. Weedbrook, D. Vitali, J. H. Shapiro, and S. Pirandola, Phys. Rev. Lett. **114**, 080503 (2015).
[5] S. Lloyd, Science **321**, 1463 (2008).
[6] H.-G. Li, D.-J. Zhang, D.-Q. Xu, Q.-L. Zhao, S. Wang, H.-B. Wang, J. Xiong, and K. Wang, Phys. Rev. A **92**, 043816 (2015).
[7] Z. Luo, J. Li, Z. Li, L.-Y. Hung, Y. Wan, X. Peng, and J. Du, Nat. Phys. **14**, 160 (2017).
[8] W. Li, C. Li, and H. Song, Phys. Rev. A **95**, 023827 (2017).
[9] V. Peano, H. G. L. Schwefel, C. Marquardt, and F. Marquardt, Phys. Rev. Lett. **115**, 243603 (2015).
[10] S. Forstner, J. Knittel, E. Sheridan, J. D. Swaim, H. Rubinsztein-Dunlop, and W. P. Bowen, Photon. Sensors **2**, 259 (2012).
[11] A. D. O'Connell, M. Hofheinz, M. Ansmann, R. C. Bialczak, M. Lenander, E. Lucero, M. Neeley, D. Sank, H. Wang, M. Weides, J. Wenner, J. M. Martinis, and A. N. Cleland, Nature (London) **464**, 697 (2010).
[12] S. Forstner, S. Prams, J. Knittel, E. D. van Ooijen, J. D. Swaim, G. I. Harris, A. Szorkovszky, W. P. Bowen, and H. Rubinsztein-Dunlop, Phys. Rev. Lett. **108**, 120801 (2012).
[13] Y. Ma, S. L. Danilishin, C. Zhao, H. Miao, W. Z. Korth, Y. Chen, R. L. Ward, and D. G. Blair, Phys. Rev. Lett. **113**, 151102 (2014).
[14] A. Pontin, M. Bonaldi, A. Borrielli, L. Marconi, F. Marino, G. Pandraud, G. A. Prodi, P. M. Sarro, E. Serra, and F. Marin, Phys. Rev. A **97**, 033833 (2018).
[15] P. Meystre and M. O. Scully, *Quantum Optics, Experimental Gravity, and Measurement Theory* (Plenum, New York, 1983).
[16] M. H. Wimmer, D. Steinmeyer, K. Hammerer, and M. Heurs, Phys. Rev. A **89**, 053836 (2014).
[17] X. Huang, E. Zeuthen, D. V. Vasilyev, Q. He, K. Hammerer, and E. S. Polzik, Phys. Rev. Lett. **121**, 103602 (2018).
[18] T. Caniard, P. Verlot, T. Briant, P.-F. Cohadon, and A. Heidmann, Phys. Rev. Lett. **99**, 110801 (2007).
[19] A. Motazedifard, F. Bemani, M. H. Naderi, R. Roknizadeh, and D. Vitali, New J. Phys. **18**, 073040 (2016).
[20] H. Miao, Y. Ma, C. Zhao, and Y. Chen, Phys. Rev. Lett. **115**, 211104 (2015).
[21] F. Lecocq, J. B. Clark, R. W. Simmonds, J. Aumentado, and J. D. Teufel, Phys. Rev. X **5**, 041037 (2015).
[22] B. Xiong, X. Li, X.-Y. Wang, and L. Zhou, Ann. Phys. **385**, 757 (2017).
[23] S. Barzanjeh, E. S. Redchenko, M. Peruzzo, M. Wulf, D. P. Lewis, G. Arnold, and J. M. Fink, arXiv:1809.05865.
[24] C. F. Ockeloen-Korppi, E. Damskägg, J.-M. Pirkkalainen, M. Asjad, A. A. Clerk, F. Massel, M. J. Woolley, and M. A. Sillanpää, Nature (London) **556**, 478 (2018).
[25] A. Pontin, J. E. Lang, A. Chowdhury, P. Vezio, F. Marino, B. Morana, E. Serra, F. Marin, and T. S. Monteiro, Phys. Rev. Lett. **120**, 020503 (2018).
[26] M. Aspelmeyer, T. J. Kippenberg, and F. Marquardt, Rev. Mod. Phys. **86**, 1391 (2014).
[27] F. Bariani, H. Seok, S. Singh, M. Vengalattore, and P. Meystre, Phys. Rev. A **92**, 043817 (2015).
[28] Y. S. Patil, S. Chakram, L. Chang, and M. Vengalattore, Phys. Rev. Lett. **115**, 017202 (2015).
[29] M. Schaffry, E. M. Gauger, J. J. L. Morton, and S. C. Benjamin, Phys. Rev. Lett. **107**, 207210 (2011).
[30] X. Xu and J. M. Taylor, Phys. Rev. A **90**, 043848 (2014).
[31] A. A. Clerk, F. Marquardt, and K. Jacobs, New J. Phys. **10**, 095010 (2008).

[32] J. D. Teufel, T. Donner, D. Li, J. W. Harlow, M. S. Allman, K. Cicak, A. J. Sirois, J. D. Whittaker, K. W. Lehnert, and R. W. Simmonds, Nature (London) **475**, 359 (2011).

[33] K. Zhang, F. Bariani, Y. Dong, W. Zhang, and P. Meystre, Phys. Rev. Lett. **114**, 113601 (2015).

[34] A. Castellanos-Gomez, H. B. Meerwaldt, W. J. Venstra, H. S. J. van der Zant, and G. A. Steele, Phys. Rev. B **86**, 041402(R) (2012).

[35] J. R. Johansson, N. Lambert, I. Mahboob, H. Yamaguchi, and F. Nori, Phys. Rev. B **90**, 174307 (2014).

[36] M. Cirio, K. Debnath, N. Lambert, and F. Nori, Phys. Rev. Lett. **119**, 053601 (2017).

[37] M. J. Seitner, M. Abdi, A. Ridolfo, M. J. Hartmann, and E. M. Weig, Phys. Rev. Lett. **118**, 254301 (2017).

[38] H. Okamoto, A. Gourgout, C.-Y. Chang, K. Onomitsu, I. Mahboob, E. Y. Chang, and H. Yamaguchi, Nat. Phys. **9**, 480 (2013).

[39] P. Huang, L. Zhang, J. Zhou, T. Tian, P. Yin, C. Duan, and J. Du, Phys. Rev. Lett. **117**, 017701 (2016).

[40] D.-G. Lai, F. Zou, B.-P. Hou, Y.-F. Xiao, and J.-Q. Liao, Phys. Rev. A **98**, 023860 (2018).

[41] N. Spethmann, J. Kohler, S. Schreppler, L. Buchmann, and D. M. Stamper-Kurn, Nat. Phys. **12**, 27 (2016).

[42] A. Pontin, M. Bonaldi, A. Borrielli, L. Marconi, F. Marino, G. Pandraud, G. A. Prodi, P. M. Sarro, E. Serra, and F. Marin, Phys. Rev. Lett. **116**, 103601 (2016).

[43] M. Lapine, I. V. Shadrivov, D. A. Powell, and Y. S. Kivshar, Nat. Mater. **11**, 30 (2012).